PHYSICAL REVIEW C **91**, 064904 (2015)

Centrality dependence of low-momentum direct-photon production in Au + Au collisions at $\sqrt{s_{NN}} = 200$ GeV

A. Adare,[13] S. Afanasiev,[31] C. Aidala,[40,44,45] N. N. Ajitanand,[64] Y. Akiba,[58,59] R. Akimoto,[12] H. Al-Bataineh,[52] H. Al-Ta'ani,[52] J. Alexander,[64] A. Angerami,[14] K. Aoki,[36,58] N. Apadula,[65] Y. Aramaki,[12,58] H. Asano,[36,58] E. C. Aschenauer,[7] E. T. Atomssa,[37,65] R. Averbeck,[65] T. C. Awes,[54] B. Azmoun,[7] V. Babintsev,[25] M. Bai,[6] G. Baksay,[20] L. Baksay,[20] B. Bannier,[65] K. N. Barish,[8] B. Bassalleck,[51] A. T. Basye,[1] S. Bathe,[5,8,59] V. Baublis,[57] C. Baumann,[46] S. Baumgart,[58] A. Bazilevsky,[7] S. Belikov,[7,*] R. Belmont,[69] R. Bennett,[65] A. Berdnikov,[61] Y. Berdnikov,[61] A. A. Bickley,[13] X. Bing,[53] D. S. Blau,[35] J. S. Bok,[52,73] K. Boyle,[59,65] M. L. Brooks,[40] H. Buesching,[7] V. Bumazhnov,[25] G. Bunce,[7,59] S. Butsyk,[40,51] C. M. Camacho,[40] S. Campbell,[65] P. Castera,[65] C.-H. Chen,[65] C. Y. Chi,[14] M. Chiu,[7] I. J. Choi,[26,73] J. B. Choi,[10] S. Choi,[63] R. K. Choudhury,[4] P. Christiansen,[42] T. Chujo,[68] P. Chung,[64] O. Chvala,[8] V. Cianciolo,[54] Z. Citron,[65] B. A. Cole,[14] M. Connors,[65] P. Constantin,[40] M. Csanád,[18] T. Csörgő,[72] T. Dahms,[65] S. Dairaku,[36,58] I. Danchev,[69] K. Das,[21] A. Datta,[44] M. S. Daugherity,[1] G. David,[7] A. Denisov,[25] A. Deshpande,[59,65] E. J. Desmond,[7] K. V. Dharmawardane,[52] O. Dietzsch,[62] L. Ding,[29] A. Dion,[29,65] M. Donadelli,[62] O. Drapier,[37] A. Drees,[65] K. A. Drees,[6] J. M. Durham,[40,65] A. Durum,[25] D. Dutta,[4] L. D'Orazio,[43] S. Edwards,[6,21] Y. V. Efremenko,[54] F. Ellinghaus,[13] T. Engelmore,[14] A. Enokizono,[39,54] H. En'yo,[58,59] S. Esumi,[68] K. O. Eyser,[8] B. Fadem,[47] D. E. Fields,[51] M. Finger,[9] M. Finger, Jr.,[9] F. Fleuret,[37] S. L. Fokin,[35] Z. Fraenkel,[71,*] J. E. Frantz,[53,65] A. Franz,[7] A. D. Frawley,[21] K. Fujiwara,[58] Y. Fukao,[58] T. Fusayasu,[49] K. Gainey,[1] C. Gal,[65] A. Garishvili,[66] I. Garishvili,[39,66] A. Glenn,[13,39] H. Gong,[65] X. Gong,[64] M. Gonin,[37] Y. Goto,[58,59] R. Granier de Cassagnac,[37] N. Grau,[2,14] S. V. Greene,[69] M. Grosse Perdekamp,[26,59] T. Gunji,[12] L. Guo,[40] H.-Å. Gustafsson,[42,*] T. Hachiya,[58] J. S. Haggerty,[7] K. I. Hahn,[19] H. Hamagaki,[12] J. Hamblen,[66] R. Han,[56] J. Hanks,[14] E. P. Hartouni,[39] K. Hashimoto,[58,60] E. Haslum,[42] R. Hayano,[12] X. He,[22] M. Heffner,[39] T. K. Hemmick,[65] T. Hester,[8] J. C. Hill,[29] M. Hohlmann,[20] R. S. Hollis,[8] W. Holzmann,[14] K. Homma,[24] B. Hong,[34] T. Horaguchi,[24,68] Y. Hori,[12] D. Hornback,[66] S. Huang,[69] T. Ichihara,[58,59] R. Ichimiya,[58] J. Ide,[47] H. Iinuma,[33] Y. Ikeda,[58,68] K. Imai,[30,36,58] J. Imrek,[17] M. Inaba,[68] A. Iordanova,[8] D. Isenhower,[1] M. Ishihara,[58] T. Isobe,[12,58] M. Issah,[69] A. Isupov,[31] D. Ivanischev,[57] D. Ivanishchev,[57] B. V. Jacak,[65] M. Javani,[22] J. Jia,[7,64] X. Jiang,[40] J. Jin,[14] B. M. Johnson,[7] K. S. Joo,[48] D. Jouan,[55] D. S. Jumper,[1,26] F. Kajihara,[12] S. Kametani,[58] N. Kamihara,[59] J. Kamin,[65] S. Kaneti,[65] B. H. Kang,[23] J. H. Kang,[73] J. S. Kang,[23] J. Kapustinsky,[40] K. Karatsu,[36,58] M. Kasai,[58,60] D. Kawall,[44,59] M. Kawashima,[58,60] A. V. Kazantsev,[35] T. Kempel,[29] A. Khanzadeev,[57] K. M. Kijima,[24] B. I. Kim,[34] C. Kim,[34] D. H. Kim,[48] D. J. Kim,[32] E. Kim,[63] E.-J. Kim,[10] H. J. Kim,[73] K.-B. Kim,[10] S. H. Kim,[73] Y.-J. Kim,[26] Y. K. Kim,[23] E. Kinney,[13] K. Kiriluk,[13] Á. Kiss,[18] E. Kistenev,[7] J. Klatsky,[21] D. Kleinjan,[8] P. Kline,[65] L. Kochenda,[57] Y. Komatsu,[12] B. Komkov,[57] M. Konno,[68] J. Koster,[26] D. Kotchetkov,[51,53] D. Kotov,[57,61] A. Kozlov,[71] A. Král,[15] A. Kravitz,[14] F. Krizek,[32] G. J. Kunde,[40] K. Kurita,[58,60] M. Kurosawa,[58] Y. Kwon,[73] G. S. Kyle,[52] R. Lacey,[64] Y. S. Lai,[14] J. G. Lajoie,[29] A. Lebedev,[29] B. Lee,[23] D. M. Lee,[40] J. Lee,[19] K. Lee,[63] K. B. Lee,[34] K. S. Lee,[34] S. H. Lee,[65] S. R. Lee,[10] M. J. Leitch,[40] M. A. L. Leite,[62] M. Leitgab,[26] E. Leitner,[69] B. Lenzi,[62] B. Lewis,[65] X. Li,[11] P. Liebing,[59] S. H. Lim,[73] L. A. Linden Levy,[13] T. Liška,[15] A. Litvinenko,[31] H. Liu,[40,52] M. X. Liu,[40] B. Love,[69] R. Luechtenborg,[46] D. Lynch,[7] C. F. Maguire,[69] Y. I. Makdisi,[6] M. Makek,[71,74] A. Malakhov,[31] M. D. Malik,[51] A. Manion,[65] V. I. Manko,[35] E. Mannel,[14] Y. Mao,[56,58] H. Masui,[68] S. Masumoto,[12] F. Matathias,[14] M. McCumber,[13,65] P. L. McGaughey,[40] D. McGlinchey,[13,21] C. McKinney,[26] N. Means,[65] M. Mendoza,[8] B. Meredith,[26] Y. Miake,[68] T. Mibe,[33] A. C. Mignerey,[43] P. Mikeš,[9,28] K. Miki,[58,68] A. Milov,[7,71] D. K. Mishra,[4] M. Mishra,[3] J. T. Mitchell,[7] Y. Miyachi,[58,67] S. Miyasaka,[58,67] A. K. Mohanty,[4] H. J. Moon,[48] Y. Morino,[12] A. Morreale,[8] D. P. Morrison,[7,†] S. Motschwiller,[47] T. V. Moukhanova,[35] T. Murakami,[36,58] J. Murata,[58,60] T. Nagae,[36] S. Nagamiya,[33,58] J. L. Nagle,[13,‡] M. Naglis,[71] M. I. Nagy,[18,72] I. Nakagawa,[58,59] Y. Nakamiya,[24] K. R. Nakamura,[36,58] T. Nakamura,[33,58] K. Nakano,[58,67] C. Nattrass,[66] A. Nederlof,[47] J. Newby,[39] M. Nguyen,[65] M. Nihashi,[24,58] R. Nouicer,[7,59] N. Novitzky,[32] A. S. Nyanin,[35] E. O'Brien,[7] S. X. Oda,[12] C. A. Ogilvie,[29] M. Oka,[68] K. Okada,[59] Y. Onuki,[58] A. Oskarsson,[42] M. Ouchida,[24,58] K. Ozawa,[12] R. Pak,[7] V. Pantuev,[27,65] V. Papavassiliou,[52] B. H. Park,[23] I. H. Park,[19] J. Park,[63] S. K. Park,[34] W. J. Park,[34] S. F. Pate,[52] L. Patel,[22] H. Pei,[29] J.-C. Peng,[26] H. Pereira,[16] V. Peresedov,[31] D.Yu. Peressounko,[35] R. Petti,[7,65] C. Pinkenburg,[7] R. P. Pisani,[7] M. Proissl,[65] M. L. Purschke,[7] A. K. Purwar,[40] H. Qu,[1,22] J. Rak,[32] A. Rakotozafindrabe,[37] I. Ravinovich,[71] K. F. Read,[54,66] K. Reygers,[46] D. Reynolds,[64] V. Riabov,[50,57] Y. Riabov,[57,61] E. Richardson,[43] N. Riveli,[53] D. Roach,[69] G. Roche,[41,*] S. D. Rolnick,[8] M. Rosati,[29] C. A. Rosen,[13] S. S. E. Rosendahl,[42] P. Rosnet,[41] P. Rukoyatkin,[31] P. Ružička,[28] B. Sahlmueller,[46,65] N. Saito,[33] T. Sakaguchi,[7] K. Sakashita,[58,67] V. Samsonov,[50,57] M. Sano,[68] S. Sano,[12,70] M. Sarsour,[22] T. Sato,[68] S. Sawada,[33] K. Sedgwick,[8] J. Seele,[13] R. Seidl,[26,58,59] A.Yu. Semenov,[29] A. Sen,[22] R. Seto,[8] D. Sharma,[71] I. Shein,[25] T.-A. Shibata,[58,67] K. Shigaki,[24] M. Shimomura,[68] K. Shoji,[36,58] P. Shukla,[4] A. Sickles,[7] C. L. Silva,[29,62] D. Silvermyr,[54] C. Silvestre,[16] K. S. Sim,[34] B. K. Singh,[3] C. P. Singh,[3] V. Singh,[3] M. Slunečka,[9] R. A. Soltz,[39] W. E. Sondheim,[40] S. P. Sorensen,[66] M. Soumya,[64] I. V. Sourikova,[7] N. A. Sparks,[1] P. W. Stankus,[54] E. Stenlund,[42] M. Stepanov,[44] A. Ster,[72] S. P. Stoll,[7] T. Sugitate,[24] A. Sukhanov,[7] J. Sun,[65] J. Sziklai,[72] E. M. Takagui,[62] A. Takahara,[12] A. Taketani,[58,59] R. Tanabe,[68] Y. Tanaka,[49] S. Taneja,[65] K. Tanida,[36,58,59,63] M. J. Tannenbaum,[7] S. Tarafdar,[3] A. Taranenko,[50,64] P. Tarján,[17] E. Tennant,[52] H. Themann,[65] T. L. Thomas,[51] T. Todoroki,[58,68] M. Togawa,[36,58] A. Toia,[65] L. Tomášek,[28] M. Tomášek,[15,28] H. Torii,[24] R. S. Towell,[1] I. Tserruya,[71] Y. Tsuchimoto,[12,24] T. Tsuji,[12] C. Vale,[7,29] H. Valle,[69] H. W. van Hecke,[40] M. Vargyas,[18] E. Vazquez-Zambrano,[14] A. Veicht,[14,26] J. Velkovska,[69] R. Vértesi,[17,72] A. A. Vinogradov,[35] M. Virius,[15] A. Vossen,[26] V. Vrba,[15,28] E. Vznuzdaev,[57] X. R. Wang,[52] D. Watanabe,[24] K. Watanabe,[68] Y. Watanabe,[58,59] Y. S. Watanabe,[12] F. Wei,[29]

R. Wei,[64] J. Wessels,[46] S. Whitaker,[29] S. N. White,[7] D. Winter,[14] S. Wolin,[26] J. P. Wood,[1] C. L. Woody,[7] R. M. Wright,[1] M. Wysocki,[13] W. Xie,[59] Y. L. Yamaguchi,[12,58] K. Yamaura,[24] R. Yang,[26] A. Yanovich,[25] J. Ying,[22] S. Yokkaichi,[58,59] Z. You,[40,56] G. R. Young,[54] I. Younus,[38,51] I. E. Yushmanov,[35] W. A. Zajc,[14] A. Zelenski,[6] C. Zhang,[54] S. Zhou,[11] and L. Zolin[31]
(PHENIX Collaboration)

[1]*Abilene Christian University, Abilene, Texas 79699, USA*
[2]*Department of Physics, Augustana College, Sioux Falls, South Dakota 57197, USA*
[3]*Department of Physics, Banaras Hindu University, Varanasi 221005, India*
[4]*Bhabha Atomic Research Centre, Bombay 400 085, India*
[5]*Baruch College, City University of New York, New York, New York, 10010*
and The Graduate Center, City University of New York, New York, New York 10016, USA
[6]*Collider-Accelerator Department, Brookhaven National Laboratory, Upton, New York 11973-5000, USA*
[7]*Physics Department, Brookhaven National Laboratory, Upton, New York 11973-5000, USA*
[8]*University of California - Riverside, Riverside, California 92521, USA*
[9]*Charles University, Ovocný trh 5, Praha 1, 116 36, Prague, Czech Republic*
[10]*Chonbuk National University, Jeonju, 561-756, Korea*
[11]*Science and Technology on Nuclear Data Laboratory, China Institute of Atomic Energy, Beijing 102413, People's Republic of China*
[12]*Center for Nuclear Study, Graduate School of Science, University of Tokyo, 7-3-1 Hongo, Bunkyo, Tokyo 113-0033, Japan*
[13]*University of Colorado, Boulder, Colorado 80309, USA*
[14]*Columbia University, New York, New York 10027 and Nevis Laboratories, Irvington, New York 10533, USA*
[15]*Czech Technical University, Zikova 4, 166 36 Prague 6, Czech Republic*
[16]*Dapnia, CEA Saclay, F-91191, Gif-sur-Yvette, France*
[17]*Debrecen University, H-4010 Debrecen, Egyetem tér 1, Hungary*
[18]*ELTE, Eötvös Loránd University, H-1117 Budapest, Pázmány P. s. 1/A, Hungary*
[19]*Ewha Womans University, Seoul 120-750, Korea*
[20]*Florida Institute of Technology, Melbourne, Florida 32901, USA*
[21]*Florida State University, Tallahassee, Florida 32306, USA*
[22]*Georgia State University, Atlanta, Georgia 30303, USA*
[23]*Hanyang University, Seoul 133-792, Korea*
[24]*Hiroshima University, Kagamiyama, Higashi-Hiroshima 739-8526, Japan*
[25]*IHEP Protvino, State Research Center of Russian Federation, Institute for High Energy Physics, Protvino, 142281, Russia*
[26]*University of Illinois at Urbana-Champaign, Urbana, Illinois 61801, USA*
[27]*Institute for Nuclear Research of the Russian Academy of Sciences, prospekt 60-letiya Oktyabrya 7a, Moscow 117312, Russia*
[28]*Institute of Physics, Academy of Sciences of the Czech Republic, Na Slovance 2, 182 21 Prague 8, Czech Republic*
[29]*Iowa State University, Ames, Iowa 50011, USA*
[30]*Advanced Science Research Center, Japan Atomic Energy Agency, 2-4 Shirakata Shirane, Tokai-mura,*
Naka-gun, Ibaraki-ken 319-1195, Japan
[31]*Joint Institute for Nuclear Research, 141980 Dubna, Moscow Region, Russia*
[32]*Helsinki Institute of Physics and University of Jyväskylä, P.O.Box 35, FI-40014 Jyväskylä, Finland*
[33]*KEK, High Energy Accelerator Research Organization, Tsukuba, Ibaraki 305-0801, Japan*
[34]*Korea University, Seoul, 136-701, Korea*
[35]*Russian Research Center "Kurchatov Institute", Moscow, 123098 Russia*
[36]*Kyoto University, Kyoto 606-8502, Japan*
[37]*Laboratoire Leprince-Ringuet, Ecole Polytechnique, CNRS-IN2P3, Route de Saclay, F-91128, Palaiseau, France*
[38]*Physics Department, Lahore University of Management Sciences, Lahore 54792, Pakistan*
[39]*Lawrence Livermore National Laboratory, Livermore, California 94550, USA*
[40]*Los Alamos National Laboratory, Los Alamos, New Mexico 87545, USA*
[41]*LPC, Université Blaise Pascal, CNRS-IN2P3, F-Clermont-Fd, 63177 Aubiere Cedex, France*
[42]*Department of Physics, Lund University, Box 118, SE-221 00 Lund, Sweden*
[43]*University of Maryland, College Park, Maryland 20742, USA*
[44]*Department of Physics, University of Massachusetts, Amherst, Massachusetts 01003-9337, USA*
[45]*Department of Physics, University of Michigan, Ann Arbor, Michigan 48109-1040, USA*
[46]*Institut fur Kernphysik, University of Muenster, D-48149 Muenster, Germany*
[47]*Muhlenberg College, Allentown, Pennsylvania 18104-5586, USA*
[48]*Myongji University, Yongin, Kyonggido 449-728, Korea*
[49]*Nagasaki Institute of Applied Science, Nagasaki-shi, Nagasaki 851-0193, Japan*
[50]*National Research Nuclear University, MEPhI, Moscow Engineering Physics Institute, Moscow, 115409, Russia*
[51]*University of New Mexico, Albuquerque, New Mexico 87131, USA*
[52]*New Mexico State University, Las Cruces, New Mexico 88003, USA*

[53]*Department of Physics and Astronomy, Ohio University, Athens, Ohio 45701, USA*
[54]*Oak Ridge National Laboratory, Oak Ridge, Tennessee 37831, USA*
[55]*IPN-Orsay, Universite Paris Sud, CNRS-IN2P3, BP1, F-91406, Orsay, France*
[56]*Peking University, Beijing 100871, People's Republic of China*
[57]*PNPI, Petersburg Nuclear Physics Institute, Gatchina, Leningrad region, 188300, Russia*
[58]*RIKEN Nishina Center for Accelerator-Based Science, Wako, Saitama 351-0198, Japan*
[59]*RIKEN BNL Research Center, Brookhaven National Laboratory, Upton, New York 11973-5000, USA*
[60]*Physics Department, Rikkyo University, 3-34-1 Nishi-Ikebukuro, Toshima, Tokyo 171-8501, Japan*
[61]*Saint Petersburg State Polytechnic University, St. Petersburg, 195251 Russia*
[62]*Universidade de São Paulo, Instituto de Física, Caixa Postal 66318, São Paulo CEP05315-970, Brazil*
[63]*Department of Physics and Astronomy, Seoul National University, Seoul 151-742, Korea*
[64]*Chemistry Department, Stony Brook University, SUNY, Stony Brook, New York 11794-3400, USA*
[65]*Department of Physics and Astronomy, Stony Brook University, SUNY, Stony Brook, New York 11794-3800, USA*
[66]*University of Tennessee, Knoxville, Tennessee 37996, USA*
[67]*Department of Physics, Tokyo Institute of Technology, Oh-okayama, Meguro, Tokyo 152-8551, Japan*
[68]*Institute of Physics, University of Tsukuba, Tsukuba, Ibaraki 305, Japan*
[69]*Vanderbilt University, Nashville, Tennessee 37235, USA*
[70]*Waseda University, Advanced Research Institute for Science and Engineering, 17 Kikui-cho, Shinjuku-ku, Tokyo 162-0044, Japan*
[71]*Weizmann Institute, Rehovot 76100, Israel*
[72]*Institute for Particle and Nuclear Physics, Wigner Research Centre for Physics, Hungarian Academy of Sciences (Wigner RCP, RMKI) H-1525 Budapest 114, PO Box 49, Budapest, Hungary*
[73]*Yonsei University, IPAP, Seoul 120-749, Korea*
[74]*University of Zagreb, Faculty of Science, Department of Physics, Bijenička 32, HR-10002 Zagreb, Croatia*

(Received 23 May 2014; revised manuscript received 16 March 2015; published 5 June 2015)

The PHENIX experiment at RHIC has measured the centrality dependence of the direct photon yield from Au + Au collisions at $\sqrt{s_{NN}} = 200$ GeV down to $p_T = 0.4$ GeV/c. Photons are detected via photon conversions to e^+e^- pairs and an improved technique is applied that minimizes the systematic uncertainties that usually limit direct photon measurements, in particular at low p_T. We find an excess of direct photons above the $N_{\rm coll}$-scaled yield measured in $p + p$ collisions. This excess yield is well described by an exponential distribution with an inverse slope of about 240 MeV/c in the p_T range 0.6–2.0 GeV/c. While the shape of the p_T distribution is independent of centrality within the experimental uncertainties, the yield increases rapidly with increasing centrality, scaling approximately with $N_{\rm part}^{\alpha}$, where $\alpha = 1.38 \pm 0.03({\rm stat}) \pm 0.07({\rm syst})$.

DOI: 10.1103/PhysRevC.91.064904 PACS number(s): 25.75.Dw

I. INTRODUCTION

Photons are an excellent probe of the hot and dense, strongly interacting matter produced in heavy ion collisions [1]. They do not participate in the strong interaction and thus exit the system carrying information from the time of their emission, allowing a glimpse at the time evolution of the matter. Experimentally we measure a time-integrated history of the emission. Photons from hadron decays need to be removed to reveal the so-called direct contribution, i.e., photons that are produced before the formation of the matter as well as from the matter itself. Further removal of the early component, usually considered prompt production from $2 \rightarrow 2$ scattering of the partons from the incoming nuclei, gives access to the radiation emitted from the matter. If the matter is in local equilibrium the photon spectrum is a time-integrated image of the evolution of the temperature and collective motion of the matter as it expands and cools.

PHENIX discovered evidence of thermal photons from Au + Au collisions at the Relativistic Heavy Ion Collider (RHIC) [2]; similar findings have recently been reported by ALICE from Pb + Pb collisions at the Large Hadron Collider [3]. Photons in both energy regimes exhibit a large yield and an azimuthal anisotropy [4,5] with respect to the reaction plane, often referred to as elliptic flow and quantified as v_2. Comparing the measured p_T spectra to model calculations of thermal photons based on a hydrodynamic evolution of the system, microscopic transport models, or a more schematic time evolution gives reasonable agreement when assuming an initial temperature of 300 MeV or above [6–13] for $\sqrt{s_{NN}} = 200$ GeV Au + Au collisions at RHIC. However, it is a challenge for these types of models to simultaneously explain the large observed azimuthal anisotropy of the radiation and the large yield [13–17].

The challenge for these model calculations results from the interplay between the time evolution of the collective motion and the cooling of the matter that emits photons. In the model calculations, the collective motion builds up over time. The flow velocity is initially small and increases throughout the collision as the matter continues to expand. The yield of thermal photons is expected to be largest early in

*Deceased.
†PHENIX Co-Spokesperson: morrison@bnl.gov
‡PHENIX Co-Spokesperson: jamie.nagle@colorado.edu

the collision when the matter is the hottest. Theoretical models that create large photon v_2 typically underestimate the direct photon yield. Attempts to improve hydrodynamic models by implementing next-to-leading-order thermal rates [18], initial state fluctuations [13], formation time effects [17], increased radial flow, and enhanced coupling at T_C [16], fail to reconcile yield and anisotropy.

To resolve this puzzle, new production mechanisms have been proposed. Some enhance the thermal yield in the presence of the strong magnetic field perpendicular to the reaction plane, which creates a large anisotropy [19,20]. Other new mechanisms, such as synchrotron radiation [21] at the plasma boundary or photon production in a glasma phase [22], create an anisotropy from the initial geometry of the overlap region.

In this paper we present the first measurement of low momentum real direct photons from Au + Au collisions at 200 GeV center-of-mass energy. This measurement compliments earlier measurements of direct photons that were obtained by extrapolating low mass virtual photons to the real photon point [2]. We are able to extend the p_T range down to 0.4 GeV/c and provide new information on the centrality dependence of the direct photon yield. In particular, the centrality dependence holds the promise of helping to distinguish between different production mechanisms [23].

II. EXPERIMENT

To measure direct photons, we analyzed large data samples of 1.4×10^9 and 2.6×10^9 minimum-bias Au + Au collisions recorded with the PHENIX central arm spectrometers during the 2007 and 2010 runs, respectively. The main PHENIX detector is described in detail elsewhere [24]. In addition, a hadron blind detector (HBD) [25] was installed, except for part of the 2007 RHIC run when only one half of the HBD was installed. The data were taken with a special field configuration which essentially cancels the magnetic field around the beam axis out to about 50 cm.

Minimum-bias events were triggered using the beam-beam counters (BBC) that cover the rapidity region $3.1 < |\eta| < 3.9$ and 2π in azimuth in both beam directions. The BBC information is used to limit the vertex in beam direction to ±10 cm around the nominal position. The charge measured in the BBC is used to categorize the event centrality. The sample is divided into four centrality classes, 0%–20% for the most central selection, 20%–40%, 40%–60%, and 60%–92% for the most peripheral sample.

The raw inclusive photon yield $N_\gamma^{\rm incl}$ is measured through photon conversions to e^+e^- pairs in the detector material, which allows us to avoid hadron contamination and measure photons down to $p_T^{ee} = 0.4\,{\rm GeV}/c$. Trajectories and momenta of e^+ and e^- are determined using the drift chambers and the pad chambers that measure the deflection in the axial magnetic field together with the interaction vertex location. We require a minimum p_T of $200\,{\rm MeV}/c$. The energy is determined with the electromagnetic calorimeter (EMCal). The e^+ and e^- are identified utilizing the ring-imaging Čerenkov detector by requiring a minimum of three phototubes associated with both charged tracks at the expected ring radius as well as requiring the respective energy/momentum ratios to be greater than 0.6.

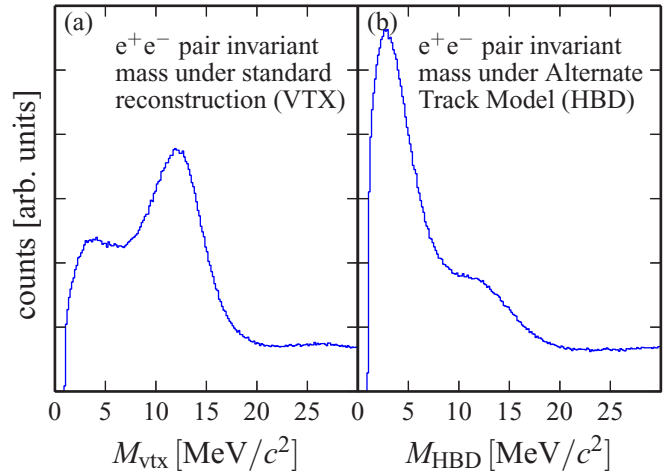

FIG. 1. (Color online) Histograms of the e^+e^- pair invariant-mass distribution from data. (a) The distribution of masses calculated with the normal reconstruction algorithm (vtx). (b) The distribution of masses calculated with the alternate track model assumption (HBD).

III. DATA ANALYSIS

We select photons that converted in the readout plane of the HBD that is located at a radius of 60 cm and has a radiation length $X/X_0 \approx 2.5\%$. Our method to identify photon conversions uses only the PHENIX central arm detectors, with the HBD playing no active role. Because the draft chambers are located at ≈220 cm radially from the beam axis, the momentum reconstruction algorithm needs to assume where the particles originate. In the standard algorithm all charged particles are reconstructed as if they came from the event vertex. This procedure mismeasures the momentum vector for e^+ and e^- from photon conversions in the HBD. For conversions in the HBD readout plane the artificial opening angle of the e^+e^- pair is ≈10 mrad and the pair momentum increases by 1%–2%. As a result the e^+e^- pair is reconstructed with an average mass of $M_{\rm vtx} \approx 12\,{\rm MeV}/c^2$, as is shown in the invariant-pair-mass distribution of Fig. 1(a). The first peak in the mass plot at a few ${\rm MeV}/c^2$ is from π^0 Dalitz decays, along with a small number of pairs from photon conversions before the HBD readout plane.

The momenta of all low mass e^+e^- pairs are recalculated assuming that they originated at the HBD readout plane. If the e^+e^- pair is indeed a conversion pair from the readout plane, the relative momentum resolution of the pair is approximately $\sigma_{p_T}^{ee}/p_T^{ee} = 0.9\% \oplus 0.5\% p_T^{ee}$ and the e^+e^- pair mass recalculated with the HBD back plane as origin ($M_{\rm HBD}$) is a few ${\rm MeV}/c^2$, consistent with the experimental resolution. For all other e^+e^- pairs, the momentum vectors are now mismeasured, in particular e^+e^- pairs from π^0 Dalitz decays are now reconstructed with larger opening angles and thus shifted upward in e^+e^- pair mass. The recalculated mass spectrum is shown in Fig. 1(b). Plotting the yield as a function of $M_{\rm HBD}$ versus the mass calculated with the vertex as origin ($M_{\rm vtx}$), as shown in Fig. 2, allows one to clearly isolate the conversions in the HBD readout plane. We select photon conversions by a two-dimensional cut

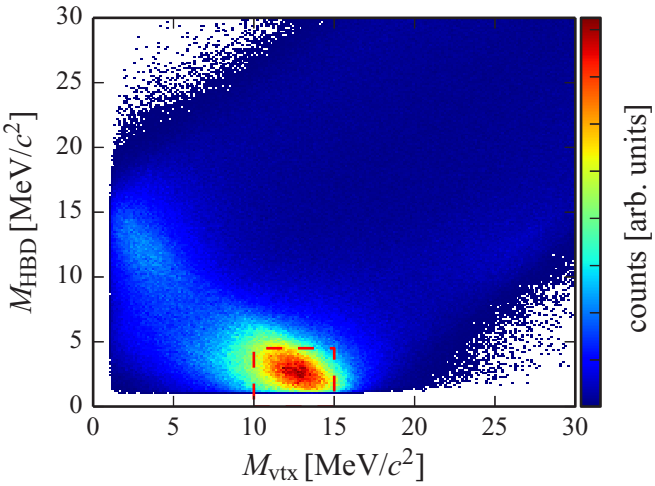

FIG. 2. (Color online) A view of the cut space used for the conversion photon identification. The mass as calculated under the standard reconstruction algorithm (vtx) is plotted on the horizontal axis, while the mass as calculated under the alternate track model (HBD) is plotted on the vertical axis. The dotted (red) box indicates the region used to identify photon conversions.

$10 < M_{\rm vtx} < 15$ MeV/c^2 and $M_{\rm HBD} < 4.5$ MeV/c^2, illustrated by the red dashed box. Note that the large distance from the true event vertex and the relatively thick HBD readout plane (in terms of radiation length X_0) with no comparable radiating material nearby makes identification of the converted photons very accurate: A full GEANT Monte Carlo simulation [26] shows that the purity of this sample is 99%, with most of the remaining 1% being photon conversions at other radii.

A subset of this inclusive conversion photon sample $N_\gamma^{\rm incl}$ is tagged statistically as photons from π^0 decays if they reconstruct the π^0 mass with a second, photonlike shower taken from the EMCal. Note that this is done in bins of p_T^{ee}, the transverse momentum of the converted photons, not in bins of $\pi^0 p_T$. A cut on the shower shape of this second EMCal shower is used to remove most hadrons. False tagging from hadron showers in the EMCal is further reduced by applying a lower threshold on the cluster energy. For the 2010 data we applied an $E_{\rm clus} > 0.4$ GeV cut, which is just above the EMCal response for minimum ionizing particles. For the 2007 data, a higher threshold of 0.6 GeV was necessary because of a cut on the shower energy that was introduced during data production.

A. Relative photon yield

In each p_T^{ee} bin the number of π^0 tagged photons ($N_\gamma^{\pi^0,{\rm tag}}$) is determined by integrating the $e^+e^-\gamma$ mass distribution around the π^0 mass after subtraction of the mixed-event combinatorial background. Figure 3 shows the mass distributions before and after subtracting the mixed-event background for two sample p_T^{ee} bins (0.4–0.6 GeV/c and 1.8–2.0 GeV/c) for central collisions (0%–20%), which have the smallest signal-to-background ratio. The π^0 peak extraction method has less than 4% systematic uncertainty on the π^0 tagged photon yield,

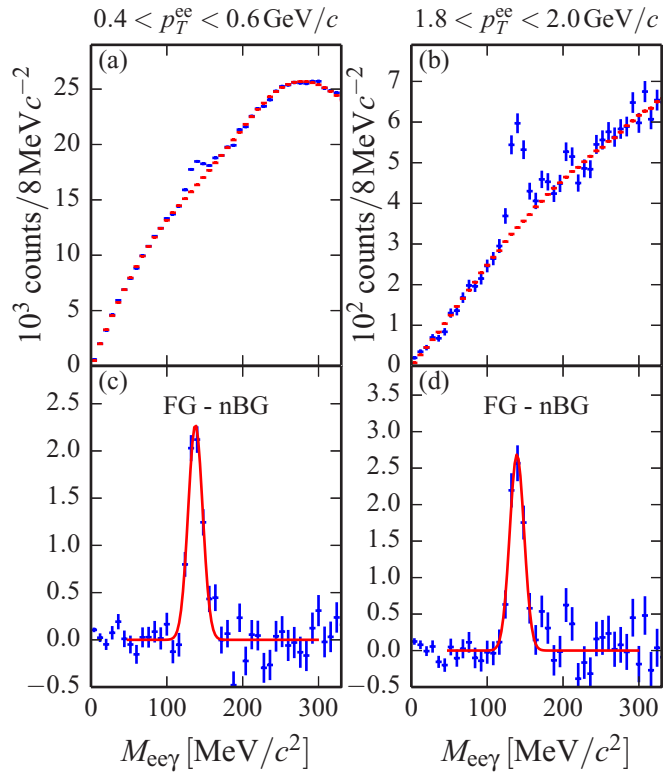

FIG. 3. (Color online) Histograms of the $e^+e^-\gamma$ invariant-mass distributions for two different p_T^{ee} bins. The left column (a) and (c) displays the mass for $0.4 < p_T^{ee} < 0.6$ GeV/c; the right column (b) and (d) displays the mass for $1.8 < p_T^{ee} < 2.0$ GeV/c. The top row (a) and (b) shows the $e^+e^-\gamma$ invariant-mass foreground distribution in blue, with the normalized background distribution from the mixed events in red. The bottom row (c) and (d) shows the isolated pion peak after subtraction of the normalized background. The masses are calculated from the HBD readout plane origin assumption on the electron tracks. The centrality bin is 0%–20%.

which is assumed to be independent between neighboring p_T^{ee} bins and thus folded into the statistical uncertainties.

In a given p_T^{ee} bin the true number of inclusive photons $\gamma^{\rm incl}$ and photons from π^0 decays γ^{π^0} are related to the measured quantities $N_\gamma^{\rm incl}$ and $N_\gamma^{\pi^0,{\rm tag}}$ as follows:

$$N_\gamma^{\rm incl} = \varepsilon_{ee} a_{ee}\, c\gamma^{\rm incl}, \tag{1}$$

$$N_\gamma^{\pi^0,{\rm tag}} = \varepsilon_{ee} a_{ee}\, c\langle\varepsilon_\gamma f\rangle\gamma^{\pi^0}, \tag{2}$$

where c is the probability that the photon converts in the HBD readout plane, ε_{ee} is the reconstruction efficiency of the e^+e^- pair, and a_{ee} is the factor describing that both e^+ and e^- are in the detector acceptance. The factor f is the conditional acceptance that after one photon from a π^0 decay was reconstructed as the e^+e^- conversion pair, the partner photon falls into the acceptance of the EMCal. The probability that the partner photon is reconstructed is given as ε_γ. The product $\varepsilon_\gamma f$ is averaged over all possible p_T of the partner photon, indicated by $\langle\varepsilon_\gamma f\rangle$.

Because $N_\gamma^{\rm incl}$ and $N_\gamma^{\pi^0,{\rm tag}}$ are both measured in terms of the p_T^{ee} of the converted photon, the efficiency and acceptance

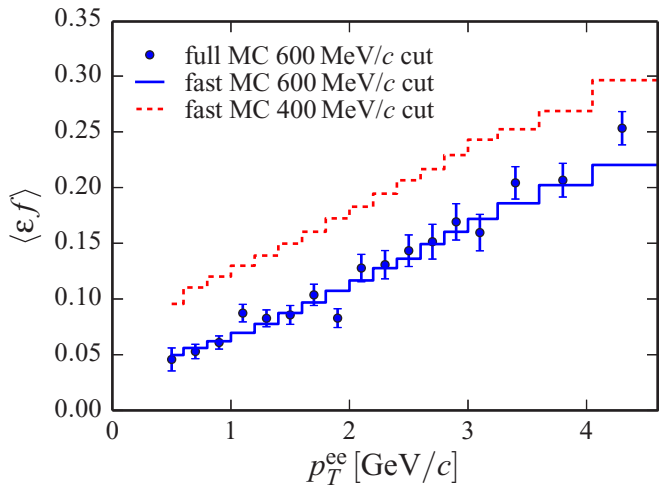

FIG. 4. (Color online) Average conditional acceptance $\langle \varepsilon_\gamma f \rangle$ to detect a photon from a π^0 decay in the EMCal, if the other photon converted in the HBD electronics and was reconstructed as an e^+e^- pair. The abscissa gives p_T^{ee}, the p_T of the e^+e^- pair. The p_T cut of 0.6 (2007) and 0.4 GeV/c (2004) is on the photon detected in the EMCal. For the p_T cut of 0.6 GeV/c we show the results for two methods, a full MC simulation (points) and a fast MC simulation (histogram). For the p_T cut of 0.4 GeV, the fast MC simulation is shown as a dashed histogram.

factors for the e^+e^- pair as well as the conversion probability explicitly cancel in the ratio $N_\gamma^{\rm incl}/N_\gamma^{\pi^0,{\rm tag}}$. This ratio can be converted into R_γ, the ratio of the yield of true inclusive photons $\gamma^{\rm incl}$ to the yield of true photons from hadron decays $\gamma^{\rm hadron}$:

$$R_\gamma = \frac{\gamma^{\rm incl}}{\gamma^{\rm hadron}} = \frac{\langle \varepsilon_\gamma f \rangle \left(\frac{N_\gamma^{\rm incl}}{N_\gamma^{\pi^0,{\rm tag}}}\right)_{\rm Data}}{\left(\frac{\gamma^{\rm hadron}}{\gamma^{\pi^0}}\right)_{\rm Sim}}. \quad (3)$$

All terms in Eq. (3) are a function of converted photon p_T^{ee}. R_γ will be unity for a given p_T^{ee} bin if all photons result from hadron decays, or larger than unity if direct photons are present in the sample. The excess above unity is a measure of the direct photon content in the bin. In the following we discuss all terms in detail.

The numerator of Eq. (3) includes the measured ratio $N_\gamma^{\rm incl}/N_\gamma^{\pi^0,{\rm tag}}$, and the efficiency and acceptance correction for pion tagging $\langle \varepsilon_\gamma f \rangle$. Figure 4 shows $\langle \varepsilon_\gamma f \rangle$ for the min. bias data sets of 2007 and 2010. It increases monotonically with p_T^{ee} and is lower for the larger p_T cut on the second photon. These trends can be understood in terms of decay kinematics and average p_T of the tagged π^0. At higher p_T^{ee} the average p_T of the tagged π^0 is larger, the opening angle between the decay photons becomes smaller, and the probability of having both decay photon in the PHENIX acceptance increases. Consequently $\langle \varepsilon_\gamma f \rangle$ increases with p_T^{ee}. A larger p_T cut on the second photon increases the minimum π^0 p_T necessary for both photons to be accepted at a given p_T^{ee}, thus $\langle \varepsilon_\gamma f \rangle$ is larger for the lower p_T cut. The ratio of $\langle \varepsilon_\gamma f \rangle$ for the two different p_T cuts is as large as a factor of 2 at the lowest p_T^{ee} and decreases towards higher p_T^{ee}. Because the final result for R_γ is proportional to $\langle \varepsilon_\gamma f \rangle$, varying the p_T cut provides a powerful cross-check for the measurement.

We developed two different methods to determine $\langle \varepsilon_\gamma f \rangle$. For the 2007 data a GEANT Monte Carlo simulation of the detector response to π^0 decays is performed. In the simulation one photon is forced to convert in the HBD readout plane. The simulated π^0 decays are then embedded into real data to account for occupancy effects in the EMCal. The events are analyzed through the full reconstruction chain to extract $\langle \varepsilon_\gamma f \rangle$. This method is computationally very intensive and thus limited by statistical uncertainties. To overcome these we developed a fast simulation. It accounts for the detector acceptance and variations of the active detector areas with time. The single photon response is parametrized based on a GEANT Monte Carlo simulation of single photons. To test the fast simulation we compared its result for $\langle \varepsilon_\gamma f \rangle$ in Fig. 4 for the 2007 data to the one determined with the full GEANT simulation; the two methods agree within statistical uncertainties. For the 2010 data we used the fast simulation. We also compare results on R_γ for p_T cuts on the second photon between 0.3 and 0.6 GeV/c^2 and find that the results are consistent well within the systematic uncertainties on $\langle \varepsilon_\gamma f \rangle$ discussed below.

The denominator of Eq. (3) is the ratio of photons from all hadron decays ($\gamma^{\rm hadron}$) to those from π^0 decays (γ^{π^0}). To evaluate this ratio, the per-event yields γ^{π^0} and $\gamma^{\rm hadron}$ are determined using the PHENIX meson decay generator EXODUS, which is discussed in detail in Ref. [27].

For each centrality class, a fit to the measured per-event yields for charged and neutral pions [28,29] is used to generate π^0's that then are decayed to photons according to known branching ratios and decay kinematics based on Ref. [30]. The resulting photon spectrum is the per-event yield γ^{π^0} as a function of photon p_T. To generate $\gamma^{\rm hadron}$, the contributions from decays of η, ω, and η' are determined using the same procedure and then added to γ^{π^0}. The shape of the p_T spectra for η, ω, and η' are derived from the π^0 spectrum by replacing p_T with $m_T = \sqrt{m_{\rm hadron}^2 - m_{\pi^0}^2 + p_T^2}$. For η and ω this is consistent with published data [31,32]; for η' no data are available. The absolute normalization of the η per-event yield is set using a value of $\eta/\pi^0 = 0.46 \pm 0.06$ [33,34] at $p_T = 5$ GeV/c. For the ω and η' the absolute yield is set to $\omega/\pi^0 = 0.9 \pm 0.06$ and $\eta'/\pi^0 = 0.25 \pm 0.075$, again at 5 GeV/$c$ (see [27]).

B. Systematic uncertainties

Several sources contribute to systematic uncertainties on $\langle \varepsilon_\gamma f \rangle$. The largest one is 4% and accounts for the uncertainties of the energy scale and the energy resolution. These translate directly into an uncertainty in the number of photons that pass the lower EMCal threshold and thus become candidates for π^0 tagging. The second largest uncertainty (2%) is on the number of photons that are lost because they convert to e^+e^- pairs in the detector material in front of the EMCal and are not reconstructed as single showers. The active area of the detectors was studied as a function of time, and the resulting systematic uncertainty on $\langle \varepsilon_\gamma f \rangle$ is smaller than 1%. Varying the π^0 input distribution with the uncertainties on

TABLE I. Summary of systematic uncertainties on R_γ. The π^0 reconstruction uncertainty is uncorrelated between data points (type A), type B uncertainties are p_T correlated, and type C are uncertainties that can change R_γ for all p_T by a constant multiplicative factor.

Source	$\sigma_{\rm syst}/R_\gamma$	Type
π^0 reconstruction		
(tagged photon yield)	4%	A
γ purity	1%	C
Conditional acceptance $\langle \varepsilon f \rangle$		
Energy scale	4%	B
Conversion loss	2%	C
γ efficiency	1%	B
Active area	1%	C
Input p_T spectra	1%	B
$\gamma^{\rm hadron}/\gamma^{\pi^0}$		
η/π^0 ratio	2.2%	C
Other mesons	<1%	C

the data results in a 1% uncertainty on $\langle \varepsilon_\gamma f \rangle$. Lastly, the uncertainty on the photon reconstruction efficiency is also small (1%), estimated by varying the shower shape cuts, redoing the analysis and recalculating the correction, and comparing the results. All other systematic effects were found to be negligible.

Systematic uncertainties on $\gamma^{\rm hadron}/\gamma^{\pi^0}$ are dominated by the accuracy with which η/π^0 is known. Because the π^0 contribution to $\gamma^{\rm hadron}$ is ≈80%, the systematic uncertainty on the π^0 spectra largely cancels, leaving the η/π^0 ratio as the dominant source of systematic uncertainties. The uncertainty on R_γ also includes possible deviations from scaling with m_T and uncertainties on the other meson yields. The total uncertainty is less than 2.5%. All systematic uncertainties on R_γ are summarized in Table I.

IV. RESULTS AND DISCUSSION

Figure 5 compares our results for R_γ in minimum-bias collisions from the 2007 and 2010 data sets separately, while Fig. 6 shows the same quantity for the four centrality selections. Here we used the full GEANT simulation for the 2007 data, and the fast Monte Carlo simulation for the 2010 data. R_γ from the two data sets agree well within statistical errors. Figure 6 also includes data from an earlier publication [2], in which R_γ was obtained by extrapolating virtual photons to $m = 0$ for the two central bins and $p_T > 1.0\,{\rm GeV}/c$. The R_γ was used to calculate the direct-photon p_T spectra shown in Ref. [2]; here we show the corresponding data points. We observe no statistically significant difference between the R_γ measured from real and virtual photons. However, given the uncertainties, we cannot rule out a difference of up to 15%, as is estimated in Ref. [12]. The R_γ shows a statistically significant excess of photons above those expected from hadron decays, and this excess increases with centrality.

To combine the data sets we apply the corrections calculated from the fast simulation for both the 2007 and 2010 data (after verifying consistency between the corrections calculated for the 2007 data with both the fast Monte Carlo and full GEANT)

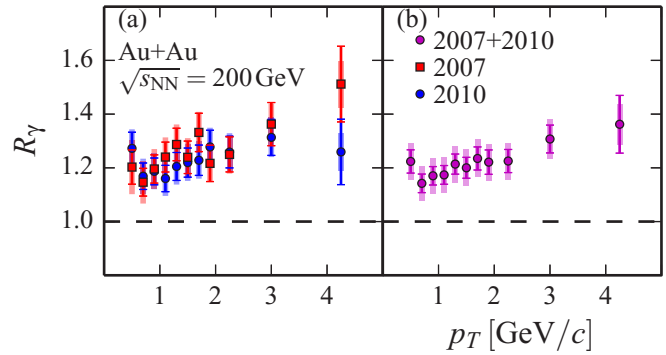

FIG. 5. (Color online) (a) Ratio R_γ as a function of photon p_T from the 2007 (red open square) and from the 2010 data sets (blue closed circle) in minimum-bias Au + Au collisions. Statistical uncertainties are dominated by the π^0 yield extraction. They are plotted as vertical lines. All other systematic uncertainties are added in quadrature and shown as filled boxes. (b) R_γ in the combined 2007+2010 measurement.

and average the numerators in Eq. (3) for the 2007 and 2010 data sets. While the correction factor $\langle \varepsilon_\gamma f \rangle$ is different for the two data sets (because of differences in detector dead areas and the different minimum photon energy cuts applied), the systematic uncertainties are the same. Next we determine the direct photon yield from the combined R_γ for each p_T bin:

$$\gamma^{\rm direct} = (R_\gamma - 1)\gamma^{\rm hadron}, \tag{4}$$

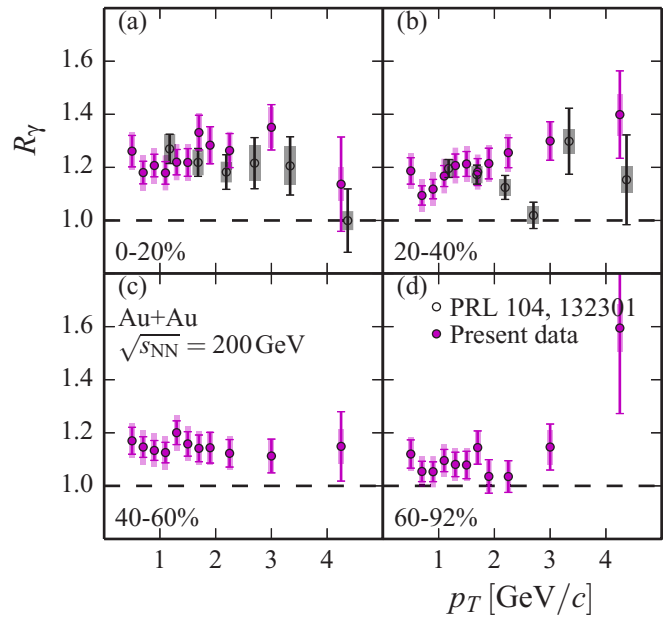

FIG. 6. (Color online) Ratio R_γ as a function of photon p_T for the combined 2007 and 2010 data sets in centrality bins 0%–20%, 20%–40%, 40%–60%, and 60%–92%. Statistical uncertainties plotted as vertical lines are dominated by the π^0 yield extraction. All other systematic uncertainties are added in quadrature and shown as filled boxes. (a) and (b) We also show earlier results from Ref. [2], obtained by extrapolating virtual photons to zero mass.

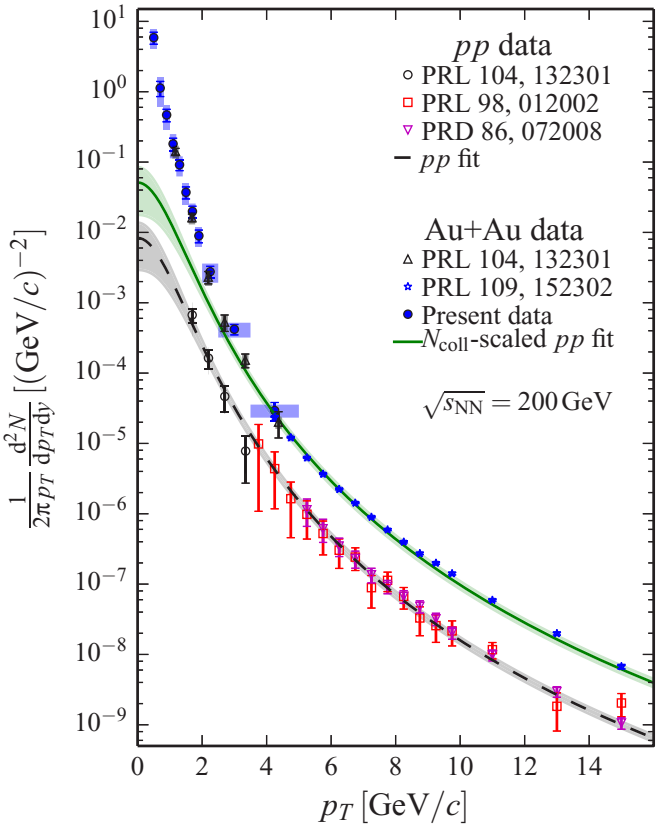

FIG. 7. (Color online) Direct photon p_T spectra for minimum-bias Au + Au collisions from this measurement (solid symbols) and Au + Au and p + p collisions (open symbols). (Open circles and up-triangles) Low p_T spectrum obtained with virtual photons in p + p and Au + Au [2]; (open squares and down-triangles) spectrum of real photons, measured in the EMCal in p + p. Open squares are 2003 data [35]; open down-triangles are 2006 data [36]. (Open stars) Spectrum with real photons, measured in the EMCal in Au + Au in 2004 [37]. The dashed line is a fit to the combined set of p + p data, extrapolated below 1 GeV/c, and the solid line the p + p fit scaled with the number of minimum-bias Au + Au collisions. Bands around lines denote 1σ uncertainty intervals in the parametrizations of the p + p data and the uncertainty in $N_{\rm coll}$, added in quadrature.

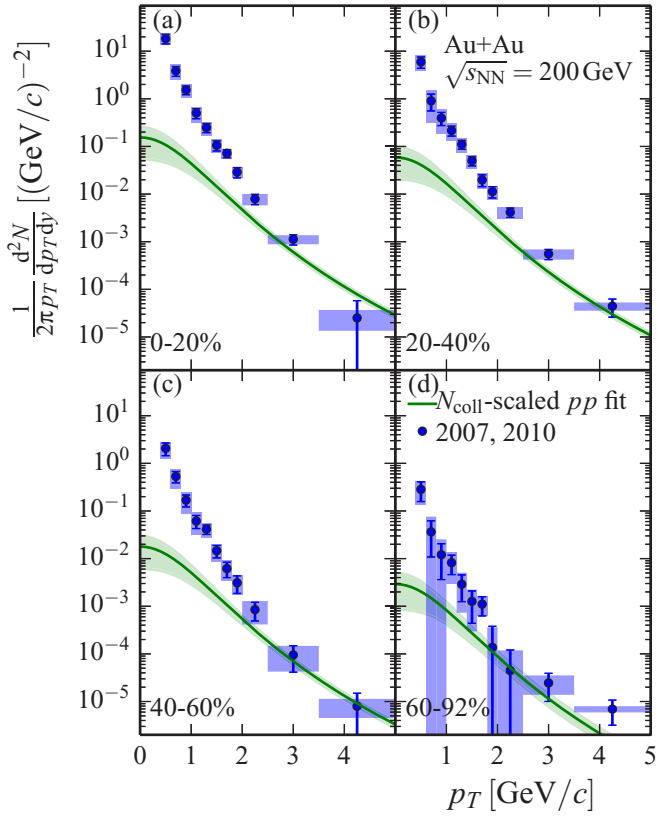

FIG. 8. (Color online) Direct photon p_T spectra in centrality bins 0%–20%, 20%–40%, 40%–60%, and 60%–92%. Widths of filled boxes indicate bin widths in this analysis. The green bands show a $N_{\rm coll}$-scaled modified power-law fit to the PHENIX p + p data and its extrapolation below 1 GeV/c; cf. Fig. 7. One-sided errors denote 1σ upper limits; other uncertainties are as in Fig. 7.

were $\gamma^{\rm hadron}$ is the invariant yield of photons from hadron decays, which we calculate from measured charged and neutral pion spectra, as described above. At this point a systematic uncertainty of 10% on the shape of the input π^0 distribution for the generator needs to be included [27] [this mostly cancels in the denominator of R_γ, but no longer cancels in Eq. (4)]. The measurement was cross-checked and found consistent with the direct photon spectrum calculated using the fully corrected measured inclusive photon spectrum [27] via the relation $\gamma^{\rm direct} = (1 - 1/R_\gamma)\gamma^{\rm incl}$, which has much larger systematic uncertainties because the conversion probability, the e^+e^- pair efficiency, and acceptance do not cancel.

Figure 7 shows the direct photon p_T spectra for minimum bias and our previously published Au + Au data from Refs. [2,37]. Also shown are the p + p photon data from PHENIX. The lowest p_T points (open circles) come from a virtual photon measurement [2], while the open squares and open triangles are from the analysis of the 2003 [35] and 2006 [36] data sets, respectively. The dashed curve is the joint fit to the p + p data with a functional form $a(1 + \frac{p_T^2}{b})^c$. This shape was used in Ref. [2]. Including new data in the fit [36], we find parameters $a = (8.3 \pm 7.5) \times 10^{-3}$, $b = 2.26 \pm 0.78$, and $c = -3.45 \pm 0.08$. Note that the systematic uncertainties are highly correlated. Also, the lowest actual data point in the fit is at $p_T = 1$ GeV/c.

The solid curve in Fig. 7 is the p + p fit scaled by the corresponding average number of binary collisions, $N_{\rm part}$, for minimum-bias collisions, as calculated from a Glauber Monte Carlo simulation [38]. Below $p_T = 3$ GeV/c, an enhancement above the expected prompt production (p + p) is observed. The enhancement has a significantly smaller inverse slope than the $N_{\rm coll}$ scaled p + p contribution.

Figure 8 shows that we observe similar behavior when investigating the centrality dependence in more detail. The solid curves are again the p + p fit scaled by the respective number of binary collisions, and they deviate significantly from the measured yields below 3 GeV/c.

Finally the direct photon contribution from prompt processes (as estimated by the $N_{\rm coll}$ scaled p + p direct photon yield, shown by the curve in Fig. 8) is subtracted to isolate

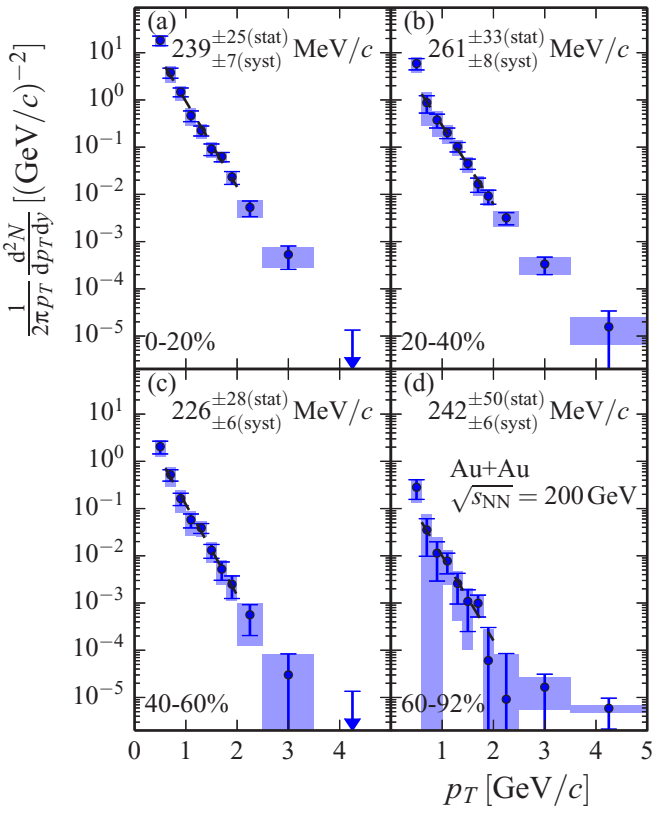

FIG. 9. (Color online) Direct photon p_T spectra after subtraction of the N_{coll} scaled $p + p$ contribution in centrality bins 0%–20%, 20%–40%, 40%–60%, and 60%–92%. Uncertainties are plotted as in Fig. 8. Dashed lines are fits to an exponential function in the range $0.6\,\text{GeV}/c < p_T < 2.0\,\text{GeV}/c$.

the radiation unique to heavy ion collisions. The results are depicted in Fig. 9. While the origin of this additional radiation cannot be directly established (it could be, for instance, thermal and/or initial state radiation, or the dominant source could even be p_T dependent), it is customary to fit this region with an exponential and characterize the shape with the inverse slope. Accordingly, shown on each panel is a fit to an exponential function in the range $0.6 < p_T < 2\,\text{GeV}/c$. The inverse slopes are approximately $240\,\text{MeV}/c$ independent of centrality; see Table II. In contrast, the yield clearly increases with centrality. We have quantified this by integrating the photon yield above a

TABLE II. The number of nucleon participants N_{part}, number of binary nucleon-nucleon collisions N_{coll}, and constituent-quark participants N_{qp} vs centrality bin. Also shown are the values of local inverse slopes in the p_T range 0.6–2 GeV/c of the direct photon spectra, after subtracting the N_{coll} scaled $p + p$ results.

Centrality	N_{coll}	N_{part}	N_{qp}	T_{eff} (MeV/c)
0%–20%	770.6 ± 79.9	277.5 ± 6.5	735.2 ± 14.6	$239 \pm 25 \pm 7$
20%–40%	282.4 ± 28.4	135.6 ± 7.0	333.2 ± 10.7	$260 \pm 33 \pm 8$
40%–60%	82.6 ± 9.3	56.0 ± 5.3	126.6 ± 6.1	$225 \pm 28 \pm 6$
60%–92%	12.1 ± 3.1	12.5 ± 2.6	25.8 ± 4.0	$238 \pm 50 \pm 6$
0%–92%	251.1 ± 26.7	106.3 ± 5.0	268.8 ± 8.2	$242 \pm 28 \pm 7$

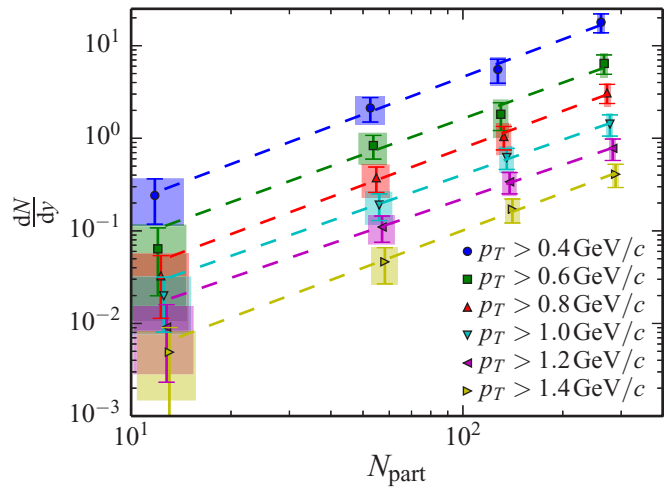

FIG. 10. (Color online) Integrated thermal photon yields as a function of N_{part} for different lower p_T integration limits. The dashed lines are independent fits to a power law.

threshold p_T^{min}. We varied the threshold from 0.4 to $1.4\,\text{GeV}/c$ to show that the centrality dependence does not result from a change of shape at low p_T (see Fig. 10).

The yield increases with a power-law function N_{part}^{α}; this is illustrated by the linear rise of the yield with N_{part} in the logarithmic representation shown on Fig. 10 together with fits to $AN_{\text{part}}^{\alpha}$. The fit parameters are shown in Table III. The same power is observed independent of the p_T cutoff, consistent with the spectra having the same shape independent of centrality. A simultaneous fit to the data in Fig. 10 results in an average value of $\alpha = 1.38 \pm 0.03(\text{stat}) \pm 0.07(\text{syst})$.

We have also considered the recently suggested scaling with the number of quark participants N_{qp}, which works well for charged particle production [39]. Here N_{qp} is calculated with a Glauber Monte Carlo simulation similar to N_{part} by picking random locations for constituent quarks within the nucleus. While our data are better described by scaling with a power law in N_{part}, they are also consistent with a power-law function N_{qp}^{β}, where N_{qp} is the number of quark participants. In this case we find an exponent of $\beta = 1.27 \pm 0.03(\text{stat}) \pm 0.07(\text{syst})$.

In most theoretical models thermal photon emission involves binary collisions of constituents, partons or hadrons, in hot and dense matter. Thus the emission rate from a unit volume should be proportional to the square of the number of constituents, while bulk particle production should scale

TABLE III. Fitted parameters from fitting power-law fits $\frac{dN}{dy} = AN_{\text{part}}^{\alpha}$ for integrated yields with different lower p_T^{ee} limits.

p_T^{min} (GeV/c)	α	A
0.4	$1.36 \pm 0.08 \pm 0.08$	$(7.85 \pm 2.96 \pm 4.52) \times 10^{-3}$
0.6	$1.41 \pm 0.14 \pm 0.12$	$(2.20 \pm 1.54 \pm 1.64) \times 10^{-3}$
0.8	$1.42 \pm 0.07 \pm 0.11$	$(1.07 \pm 0.39 \pm 0.75) \times 10^{-3}$
1.0	$1.35 \pm 0.06 \pm 0.07$	$(7.70 \pm 2.32 \pm 4.37) \times 10^{-4}$
1.2	$1.36 \pm 0.09 \pm 0.07$	$(3.90 \pm 1.79 \pm 2.81) \times 10^{-4}$
1.4	$1.40 \pm 0.06 \pm 0.10$	$(1.63 \pm 0.47 \pm 1.11) \times 10^{-4}$

with the number of constituents [23,40]. Because particle production is approximately proportional to $N_{\rm part}$ one might expect thermal photon emission to scale as $N_{\rm part}^2$ times a correction for the increasing reaction volume with centrality. The increasing volume will reduce the centrality dependence, so that one expects $1 < \alpha < 2$ for thermal photon emission, just as observed.

Recent theoretical studies of the centrality dependence confirm our finding that the yield of thermal photon emission increases approximately with a power-law function of $N_{\rm part}$. In the PHSD transport approach the power α is approximately 1.5 [41], with no evident change in the shape of the spectra with centrality, very similar to our data. A hydrodynamic model [42] shows a power-law increase of the yield with a power α in the range from 1.67 to 1.9, increasing monotonically as the lower integration threshold increases from 0.4 to 1.4 GeV/c. Photon production in a glasma phase [22] was predicted to scale with $N_{\rm part}^{\alpha}$ with $1.47 < \alpha < 2.2$. Other new production mechanisms, proposed to address the large v_2, have distinctly different centrality dependence. The yield from enhanced thermal photon emission in the strong magnetic field is expected to decrease with centrality, as the strength of the field weakens with decreasing impact parameter [19]. The thermal photon yield should thus increase more slowly than expected from standard processes, but a quantitative estimate is not yet available.

V. SUMMARY AND CONCLUSIONS

We have isolated the low-momentum direct photon yield emitted in Au + Au collisions. The shape of the p_T spectra does not depend strongly on centrality, with an average inverse slope of 240 MeV/c in the range from 0.6 to 2 GeV/c. The yield increases with centrality as $N_{\rm part}^{\alpha}$ with $\alpha \sim 1.4$. In conclusion, these results will help distinguish between different photon-production mechanisms and will constrain models of the space-time evolution of heavy ion collisions.

ACKNOWLEDGMENTS

We thank the staff of the Collider-Accelerator and Physics Departments at Brookhaven National Laboratory and the staff of the other PHENIX participating institutions for their vital contributions. We acknowledge support from the Office of Nuclear Physics in the Office of Science of the Department of Energy, the National Science Foundation, Abilene Christian University Research Council, Research Foundation of SUNY, and Dean of the College of Arts and Sciences, Vanderbilt University (USA), Ministry of Education, Culture, Sports, Science, and Technology and the Japan Society for the Promotion of Science (Japan), Conselho Nacional de Desenvolvimento Científico e Tecnológico and Fundação de Amparo à Pesquisa do Estado de São Paulo (Brazil), Natural Science Foundation of China (People's Republic of China), Croatian Science Foundation and Ministry of Science, Education, and Sports (Croatia), Ministry of Education, Youth and Sports (Czech Republic), Centre National de la Recherche Scientifique, Commissariat à l'Énergie Atomique, and Institut National de Physique Nucléaire et de Physique des Particules (France), Bundesministerium für Bildung und Forschung, Deutscher Akademischer Austausch Dienst, and Alexander von Humboldt Stiftung (Germany), Hungarian National Science Fund, OTKA, Károly Róbert University College (Hungary), Department of Atomic Energy and Department of Science and Technology (India), Israel Science Foundation (Israel), National Research Foundation of Korea of the Ministry of Science, ICT, and Future Planning (Korea), Physics Department, Lahore University of Management Sciences (Pakistan), Ministry of Education and Science, Russian Academy of Sciences, Federal Agency of Atomic Energy (Russia), VR and Wallenberg Foundation (Sweden), the US Civilian Research and Development Foundation for the Independent States of the Former Soviet Union, the Hungarian American Enterprise Scholarship Fund, and the US-Israel Binational Science Foundation.

[1] E. V. Shuryak, Quark-gluon plasma and hadronic production of leptons, photons and psions, Phys. Lett. B **78**, 150 (1978).

[2] A. Adare *et al.* (PHENIX Collaboration), Enhanced production of direct photons in Au + Au collisions at $\sqrt{s_{NN}} = 200$ GeV and implications for the initial temperature, Phys. Rev. Lett. **104**, 132301 (2010).

[3] M. Wilde (ALICE Collaboration), Measurement of direct photons in pp and pb-pb collisions with alice, Nucl. Phys. A **904**, 573c (2013).

[4] A. Adare *et al.* (PHENIX Collaboration), Observation of direct-photon collective flow in Au + Au collisions at $\sqrt{s_{NN}} =$ 200 GeV, Phys. Rev. Lett. **109**, 122302 (2012).

[5] D. Lohner (ALICE Collaboration), Measurement of direct-photon elliptic flow in Pb-Pb collisions at $\sqrt{s_{NN}} = 2.76$ TeV, J. Phys. Conf. Series **446**, 012028 (2013).

[6] D. d'Enterria and D. Peressounko, Probing the QCD equation of state with thermal photons in nucleus-nucleus collisions at RHIC, Euro. Phys. J. **46**, 451 (2006).

[7] S. Turbide, R. Rapp, and C. Gale, Hadronic production of thermal photons, Phys. Rev. C **69**, 014903 (2004).

[8] P. Huovinen, P. V. Ruuskanen, and S. S. Räsänen, Photon emission in heavy ion collisions at the cern sps, Phys. Lett. B **535**, 109 (2002).

[9] D. K. Srivastava and B. Sinha, Radiation of single photons from Pb + Pb collisions at relativistic energies and the quark-hadron phase transition, Phys. Rev. C **64**, 034902 (2001).

[10] J. Alam, S. Sarkar, T. Hatsuda, T. K. Nayak, and B. Sinha, Photons from Pb-Pb collisions at ultrarelativistic energies, Phys. Rev. C **63**, 021901(R) (2001).

[11] F. M. Liu, T. Hirano, K. Werner, and Y. Zhu, Centrality-dependent direct photon p_t spectra in Au + Au collisions at the BNL relativistic heavy ion collider (RHIC) energy $\sqrt{s_{NN}} = 200$ GeV, Phys. Rev. C **79**, 014905 (2009).

[12] K. Dusling and I. Zahed, Thermal photons from heavy ion collisions: A spectral function approach, Phys. Rev. C **82**, 054909 (2010).

[13] T. Renk, γ-hadron correlations as a tool to trace the flow of energy lost from hard partons in heavy-ion collisions, Phys. Rev. C **80**, 014901 (2009).

[14] H. Holopainen, S. S. Räsänen, and K. J. Eskola, Elliptic flow of thermal photons in heavy-ion collisions at energies available at the BNL relativistic heavy ion collider and at the CERN large hadron collider, Phys. Rev. C **84**, 064903 (2011).

[15] A. K. Chaudhuri and B. Sinha, Direct photon production from viscous quark-gluon plasma, Phys. Rev. C **83**, 034905 (2011).

[16] H. van Hees, C. Gale, and R. Rapp, Thermal photons and collective flow at energies available at the bnl relativistic heavy-ion collider, Phys. Rev. C **84**, 054906 (2011).

[17] F.-M. Liu and S.-X. Liu, Quark-gluon plasma formation time and direct photons from heavy ion collisions, Phys. Rev. C **89**, 034906 (2014).

[18] K. Kajantie, J. Kapusta, L. McLerran, and A. Mekjian, Dilepton emission and the QCD phase transition in ultrarelativistic nuclear collisions, Phys. Rev. D **34**, 2746 (1986).

[19] G. Basar, D. E. Kharzeev, and V. Skokov, Conformal anomaly as a source of soft photons in heavy ion collisions, Phys. Rev. Lett. **109**, 202303 (2012).

[20] B. Müller, S.-Y. Wu, and D.-L. Yang, Elliptic flow from thermal photons with magnetic field in holography, Phys. Rev. D **89**, 026013 (2014).

[21] V. V. Goloviznin, A. M. Snigirev, and G. M. Zinovjev, Towards azimuthal anisotropy of direct photons, J. Exp. Theor. Phys. Lett. **98**, 61 (2013).

[22] M. Chiu, T. K. Hemmick, V. Khachatryan, A. Leonidov, J. Liao, and L. McLerran, Production of photons and dileptons in the glasma, Nucl. Phys. A **900**, 16 (2013).

[23] V. Cerny, P. Lichard, and J. Pisut, A clear cut test of low mass dilepton production mechanism in hadronic collisions, Z. Phys. C **31**, 163 (1986).

[24] K. Adcox *et al.* (PHENIX Collaboration), PHENIX detector overview, Nucl. Instrum. Methods Phys. Res., Sect. A **499**, 469 (2003).

[25] W. Anderson *et al.* (PHENIX Collaboration), Design, construction, operation and performance of a hadron blind detector for the PHENIX experiment, Nucl. Instrum. Methods Phys. Res., Sect. A **646**, 35 (2011).

[26] R. Brun *et al.*, GEANT detector description and simulation tool, CERN Program Library Long Write-up W5013 (1994), http://wwwasd.web.cern.ch/wwwasd/geant/.

[27] A. Adare *et al.* (PHENIX Collaboration), Detailed measurement of the e^+e^- pair continuum in $p+p$ and Au + Au collisions at $\sqrt{s_{NN}} = 200$ GeV and implications for direct photon production, Phys. Rev. C **81**, 034911 (2010).

[28] S. S. Adler *et al.* (PHENIX Collaboration), Suppressed π^0 production at large transverse momentum in central Au + Au collisions at $\sqrt{s_{NN}} = 200$ GeV, Phys. Rev. Lett. **91**, 072301 (2003).

[29] S. S. Adler *et al.* (PHENIX Collaboration), Identified charged particle spectra and yields in Au + Au collisions at $\sqrt{s_{NN}} =$ 200 GeV, Phys. Rev. C **69**, 034909 (2004).

[30] J. Beringer *et al.* (Particle Data Group), Review of particle physics, Phys. Rev. D **86**, 010001 (2012).

[31] S. S. Adler *et al.* (PHENIX Collaboration), High transverse momentum. meson production in $p+p$, $d+$Au, and Au + Au collisions at $\sqrt{s_{NN}} = 200$ GeV, Phys. Rev. C **75**, 024909 (2007).

[32] A. Adare *et al.* (PHENIX Collaboration), Production of mesons in $p+p$, $d+$Au, Cu + Cu, and Au + Au collisions at $\sqrt{s_{NN}} =$ 200 GeV, Phys. Rev. C **84**, 044902 (2011).

[33] S. S. Adler *et al.* (PHENIX Collaboration), Common suppression pattern of η and π^0 mesons at high transverse momentum in Au + Au collisions at $\sqrt{s_{NN}} = 200$ GeV, Phys. Rev. Lett. **96**, 202301 (2006).

[34] A. Adare *et al.* (PHENIX Collaboration), Neutral pion production with respect to centrality and reaction plane in Au + Au collisions at $\sqrt{s_{NN}} = 200$ GeV, Phys. Rev. C **87**, 034911 (2013).

[35] S. S. Adler *et al.* (PHENIX Collaboration), Measurement of direct photon production in $p+p$ collisions at $\sqrt{s_{NN}} =$ 200 GeV, Phys. Rev. Lett. **98**, 012002 (2007).

[36] A. Adare *et al.* (PHENIX Collaboration), Direct photon production in $p+p$ collisions at $\sqrt{s} = 200$ GeV at midrapidity, Phys. Rev. D **86**, 072008 (2012).

[37] S. Afanasiev *et al.* (PHENIX Collaboration), Measurement of direct photons in Au + Au collisions at $\sqrt{s_{NN}} = 200$ GeV, Phys. Rev. Lett. **109**, 152302 (2012).

[38] M. L. Miller, K. Reygers, S. J. Sanders, and P. Steinberg, Glauber modeling in high energy nuclear collisions, Annu. Rev. Nucl. Part. Sci. **57**, 205 (2007).

[39] S. S. Adler *et al.* (PHENIX Collaboration), Transverse-energy distributions at midrapidity in $p+p$, $d+$Au, and Au + Au collisions at $\sqrt{s_{NN}} = 62.4$–200 GeV and implications for particle-production models, Phys. Rev. C **89**, 044905 (2014).

[40] D. Teaney and L. Yan, Second-order viscous corrections to the harmonic spectrum in heavy-ion collisions, Phys. Rev. C **89**, 014901 (2014).

[41] O. Linnyk, W. Cassing, and E. L. Bratkovskaya, Centrality dependence of the direct photon yield and elliptic flow in heavy-ion collisions at $\sqrt{s_{NN}} = 200$ GeV, Phys. Rev. C **89**, 034908 (2014).

[42] C. Shen, U. W Heinz, J.-F. Paquet, and C. Gale, Thermal photons as a quark-gluon plasma thermometer revisited, Phys. Rev. C **89**, 044910 (2014).